Received: 16 September 2021 | Accepted: 18 November 2021

DOI: 10.1111/ics.12753

International Journal of Cosmetic Science
SOCIÉTÉ FRANÇAISE DE COSMÉTOLOGIE

ORIGINAL ARTICLE

Chemically characterizing the cortical cell nano-structure of human hair using atomic force microscopy integrated with infrared spectroscopy (AFM-IR)

A. P. Fellows | **M. T. L. Casford** | **P. B. Davies**

Department of Chemistry, University of Cambridge, Cambridge, UK

Correspondence
A. P. Fellows, Department of Chemistry, University of Cambridge, Lensfield Road, CambridgeCB2 1EWUK.
Email: apf36@cam.ac.uk

Funding information
Engineering and Physical Sciences Research Council, Grant/Award Number: EP/R511870/1; Unilever, Grant/Award Number: EP/R511870/1

Abstract

Objective: The use of conventional microscopy and vibrational spectroscopy in the optical region to investigate the chemical nature of hair fibres on a nanometre scale is frustrated by the diffraction limit of light, prohibiting the spectral elucidation of nanoscale sub-structures that contribute to the bulk properties of hair. The aim of this work was to overcome this limitation and gain unprecedented chemical resolution of cortical cell nano-structure of hair.

Methods: The hybrid technique of AFM-IR, combining atomic force microscopy with an IR laser, circumvents the diffraction limit of light and achieves nanoscale chemical resolution down to the AFM tip radius. In this work, AFM-IR was employed on ultra-thin microtomed cross-sections of human hair fibres to spectrally distinguish and characterize the specific protein structures and environments within the nanoscale components of cortical cells.

Results: At first, a topographical and chemical distinction between the macrofibrils and the surrounding intermacrofibillar matrix was achieved based on 2.5 × 2.5 μm maps of cortical cell cross-sections. It was found that the intermacrofibrillar matrix has a large protein content and specific cysteine-related residues, whereas the macrofibrils showed bigger contributions from aliphatic amino acid residues and acidic-/ester-containing species (e.g. lipids). Localized spectra recorded at a spatial resolution of the order of the AFM tip radius enabled the chemical composition of each region to be determined following deconvolution of the Amide-I and Amide-II bands. This provided specific evidence for a greater proportion of α-helices in the macrofibrils and correspondingly larger contributions of β-sheet secondary structures in the intermacrofibrillar matrix, as inferred in earlier studies. Analysis of the parallel and antiparallel β-sheet structures, and of selected dominant amino acid residues, yielded further novel composition and conformation results for both regions.

Conclusion: In this work, we overcome the diffraction limit of light using atomic force microscopy integrated with IR laser spectroscopy (AFM-IR) to characterize

This is an open access article under the terms of the Creative Commons Attribution License, which permits use, distribution and reproduction in any medium, provided the original work is properly cited.
© 2021 The Authors. *International Journal of Cosmetic Science* published by John Wiley & Sons Ltd on behalf of Society of Cosmetic Scientists and Societe Francaise de Cosmetologie.

sub-micron features of the hair cortex at ultra-high spatial resolution. The resulting spectral analysis shows clear distinctions in the Amide bands in the macrofibrils and surrounding intermacrofibrillar matrix, yielding novel insight into the molecular structure and intermolecular stabilization interactions of the constituent proteins within each cortical component.

KEYWORDS

Amide Deconvolution, Atomic Force Microscopy, cortical cells, hair, Infrared Nanospectroscopy (AFM-IR), protein secondary structures

Résumé

Objectif: L'utilisation de la microscopie conventionnelle et de la spectroscopie vibratoire dans la région optique pour étudier la nature chimique des fibres capillaires à l'échelle nanométrique est limitée par la limite de diffraction de la lumière, interdisant l'élucidation spectrale des sous-structures à l'échelle nanométrique qui contribuent aux propriétés des cheveux en général. L'objectif de ce travail était de surmonter cette limitation et d'obtenir une résolution chimique sans précédent de la nanostructure cellulaire corticale des cheveux.

Méthodes: La technique hybride de l'AFM-IR, combinant la microscopie à force atomique avec un laser IR, contourne la limite de diffraction de la lumière et permet d'obtenir une résolution chimique à l'échelle nanométrique jusqu'au rayon de l'extrémité de l'AFM. Dans ce travail, l'AFM-IR a été employée sur des coupes transversales microtomes ultrafines de fibres de cheveux humains pour distinguer et caractériser sur le plan spectral les structures et environnements protéiques spécifiques au sein des composants à l'échelle nanométrique des cellules corticales.

Résultats: Tout d'abord, une distinction topographique et chimique entre les macrofibrilles et la matrice intermacrofibrillaire environnante a été obtenue à partir de cartes de 2,5 × 2,5 micromètres des coupes transversales des cellules corticales. Il a été constaté que la matrice intermacrofibrillaire avait une grande teneur en protéines et des résidus spécifiques liés à la cystéine, tandis que les macrofibrilles présentaient des contributions plus importantes provenant de résidus d'acides aminés aliphatiques et d'espèces acides/contenant des esters (p. ex. lipides). Les spectres localisés enregistrés à une résolution spatiale de l'ordre du rayon de l'extrémité AFM ont permis de déterminer la composition chimique de chaque région suite à la déconvolution des bandes Amide-I et Amide-II. Cela a apporté des preuves spécifiques pour une plus grande proportion des hélices alpha des macrofibrilles, de même que des contributions plus importantes des structures secondaires à feuillet bêta dans la matrice intermacrofibrillaire, déduites dans des études antérieures. L'analyse des structures parallèles et antiparallèles des feuillets bêta, et des résidus d'acides aminés dominants sélectionnés a donné des résultats inédits de composition et de conformation pour les deux régions.

Conclusion: Dans ce travail, nous avons surmonté la limite de diffraction de la lumière en utilisant la microscopie à force atomique intégrée à la spectroscopie laser IR (IR-AFM) pour caractériser les caractéristiques submicroniques

du cortex capillaire à une résolution spatiale ultra-élevée. L'analyse spectrale qui en résulte montre des distinctions nettes dans les bandes d'amide dans les macrofibrilles et la matrice intermacrofibrillaire environnante, ce qui apporte un éclairage nouveau sur la structure moléculaire et les interactions de stabilisation intermoléculaire des protéines constitutives dans chaque composant cortical.

INTRODUCTION

The structure of hair fibres has been the focus of much research over the last century with several techniques used to investigate their structure. [1–4] Hair fibres consist of three main regions (from innermost to outermost respectively): the medulla, the cortex, and the cuticles, shown schematically in Figure 1.[1,5–9] The medulla makes up the centre of the hair and consists of highly disordered fibrillar cells interspersed with vacuoles, therefore having a low density. [1,5,10] It can exist continuously or discontinuously and may even be completely absent (a phenomenon often related to the overall fibre thickness). [1,5,7,10] The outermost region of a hair fibre comprises the cuticle, which is formed from between 5 and 10 layers of overlapping cuticle cells, each approximately 0.5–1.0 μm thick. It has been extensively investigated. [1,5,9]

The main constituent of hair fibres of relevance to their mass, volume and associated mechanical properties, however, is the cortex, [1,6,11] which is the subject of the present study. As with the two other macroscopic regions, the physical structure of the cortex has been widely studied and consists of long, spindle-shaped and tightly packed cortical cells embedded in a cell membrane complex (CMC). [1,5,9,12] Individual cortical cells are made up of packed macrofibrils within an amorphous protein matrix, the intermacrofibrillar matrix (referred to subsequently as the Ext-matrix for brevity, Ext indicating it is external to the macrofibrils, inset to Figure 1). The macrofibrils, aligned parallel to each other like the cortical cell itself, show a similar rod-like geometry and give rise to the fibrous nature of bulk hair. [1,5,12] Macrofibrils are comprised of smaller microfibrils (also referred to as intermediate filaments) and subsequently into even smaller sub-units until ultimately reaching the fundamental coiled protein chain dimers, which exist predominantly as α-helix secondary structures. [5,12,13] There is a significant proportion of these coiled α-helix protein structures within macrofibrils and consequently also a significant propensity for tensile deformation with associated alpha–beta secondary structure transitions, which were characterized by Cao in 2002 and later by Kreplak et al. in 2004. [14,15] The α-helices of the macrofibril sub-units are held within the intramacrofibrillar matrix (referred to subsequently as the Int-matrix, Int indicating it is internal within the macrofibrils, further inset in Figure 1) with its high protein content and significant proportion of cystine, formed from two cysteine residues linked with a disulphide bond. [5,6,16–18] Like the Int-matrix, the Ext-matrix also constitutes high levels of Cys residues. However, the Ext-matrix is gel-like and known to swell in high humidity environments. This is, therefore, attributed to a fairly low proportion of intramatrix cross-linking. [6,16–18]

As the major constituent, and responsible for a significant proportion of the structural and mechanical properties of hair, quantitative characterization of the chemical

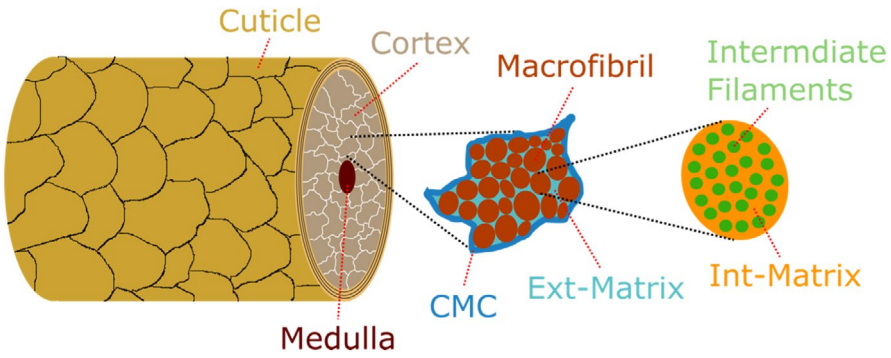

FIGURE 1 Schematic representation of the fundamental structure of a hair fibre showing the three main structural regions: the medulla, the cortex, and the cuticle. The first inset shows an enlargement of a cortical cell with its structural regions: the cell membrane complex (CMC), macrofibrils and surrounding intermacrofibrillar matrix material. The second inset shows a further enlargement of an individual macrofibril showing its sub-structure: intermediate filaments interspersed within intramacrofibrillar matrix material

and physical sub-structure of the cortex is clearly important. AFM-IR combines the localized scanning features of Atomic Force Microscopy with the chemical characterization of IR-spectroscopy in a surface selective method, providing nanoscale resolution of both IR vibrational transitions and topography. An intrinsic feature of AFM-IR is that the drawback imposed by the diffraction limit of conventional IR microscopies is eliminated, resulting in previously unachievable resolution for IR based chemical mapping. [19] Because of this, AFM-IR has proved to be a powerful analytical tool across a large variety of substrates, including many of significant relevance to biological substrates, such as red blood cells [20–23], amyloid fibrils [24], hydrogels [25], bacteria [26] and lipid monolayers [27]. Furthermore, AFM-IR was first applied to human hair cross-sections by Marcott et al. who showed the localization of structural lipids to the medulla and the CMC separating the cuticle layers. [28] More recently, AFM-IR has also been employed to analyse the layered structure of the cuticles by probing the external hair surface. [29] The current study extends this work, focussing on chemical characterization of the internal sub-structures of hair cortical cells in order to gain insight into the differential constitution of the individual components.

EXPERIMENTAL

Sample Preparation

Human hairs (European brown) from multiple individuals were first washed several times with Millipore water and rinsed with methanol. Bundles of 5 to 10 hairs were sectioned into samples 100, 200 or 300 nm thick with a diamond-tipped microtome. This provided samples where the different regions of individual hairs could be investigated as well as any hair to hair variation. Several methods of microtoming were investigated, namely, sectioning free unsupported fibres, fibres loosely supported in plastic pipette tips, and fibres held in a resin support. A cryo-ultramicrotome to freeze the fibres during microtoming was also investigated. Resin embedding of fibres for microtoming was found to be the best method for producing reliable and reproducible samples for AFM-IR. The samples were subsequently mounted without adhesive on glass coverslips for AFM-IR analysis. Spectral contributions from the resin diminished throughout the cuticle with minimal presence in the cortex, so that changes to spectroscopic and physical properties of the samples were only detectable in the 3–7 μm regions of the section perimeters. The results presented here were recorded close to the centre of the cross-section between 20 and 30 μm from the perimeter.

The predominant contribution to the AFM-IR signal at the three selected thicknesses comes from the surface layer with diminishing but finite contributions from deeper into the sample. It was established there were no contributions to the signals from the cover slips by comparing spectra from the different thicknesses and from the cover slips themselves. In fact, contributions from the surface of the cover slip are insignificant in comparison with spectral variations between the different components within the cortical cells. Furthermore, these spectral variations suggest that the contributions from deeper in the sample also maintain significant differentiation, suggesting only limited axial variability through the sample depth. This can be attributed to the fibrillar nature of the components which, because of their size in terms of both their area and depth in the sample, means they make a significant contribution to the AFM-IR spectra and represent the major component of the material axially beneath the tip. The choice of sample thickness is a compromise between maximizing the IR absorption that generates measurable cantilever deflections and maintaining a thin enough sample to resolve individual components. The IR signal-to-noise ratios at the selected thicknesses were more than sufficient to discriminate between the two structural components of interest here.

AFM-IR Analysis

Spectra and maps were recorded in contact mode using an Anasys NanoIR2 instrument equipped with a MIRcat Laser system (Daylight Solutions) containing four quantum cascade lasers (QCLs) covering the 1125–2298 cm^{-1} spectral range with transition boundaries at ~1460, 1710 and 2000 cm^{-1}. The AFM cantilever-tip assemblies used (ATEC-ContAu; Apex Probes) were gold-coated with 30-nm tip radius, approximate cone angle of ~12° (aspect ratio >4:1 over the last 1.5 μm), spring constant 0.02–0.75 Nm^{-1} and resonant frequency 7–25 kHz. An SEM image of the tip showing the approximate radius and cone geometry is given in Supplementary Information, Figure S1. Mapping was achieved with a 0.5 Hz scan rate at resolutions of at least 200 × 200 pixels. IR analysis was undertaken in resonant-enhanced mode using the second resonance frequency at ~200kHz (3% duty cycle) whilst tracking the contact resonance for mapping with a phase-lock loop (PLL). IR maps are presented here as recorded, with no background intensity correction. The laser power was varied between 3 and 11%, depending on the cross-section thickness, with the objective of optimizing the signal-to-noise ratio whilst avoiding saturating the detector. Spectra were recorded at 1 cm^{-1} per point to enable

optimum subtraction of the sharp water vapour bands and hence aid accurate spectral deconvolution.

Spectral Analysis

AFM-IR spectra were recorded under reduced humidity (dry N_2) to minimize water vapour bands that appear in the Amide-I region. The spectra were automatically background-corrected to account for environmental absorptions and variations of the laser power spectrum. Two of the QCL chip transitions occur within the regions of interest at ~1460 and 1710 cm^{-1}. The 1710 cm^{-1} transition coincides with a carbonyl absorption band and could therefore be corrected with confidence. The lower transition at 1460 cm^{-1} presented with a step-like function, probably due to the very low laser power of both chips at this frequency. Significant uncertainty must therefore arise from spectral analysis of this feature as well as when comparing intensities at frequencies either side of the transition frequency. However, as the main analysis of the different hair structures was undertaken using the Amide-I and Amide-II bands, this transition falls outside the required spectral range, thus eliminating these concerns.

Further background subtraction was then applied to remove underlying broad spectral variations using a spline curve followed by smoothing using a 7pt low-pass FFT-filter. This removed high-frequency noise contributions and had a minimum effect on any broader underlying spectral features. [30] The FFT treatment was carefully applied by comparing smoothed spectra to their raw counterparts to minimize any effect on the underlying spectral features. The same spectral procedure has been used previously on AFM-IR spectra of hair fibres where a comparison of the as-recorded and processed spectra was made and no significant alteration to the underlying spectral intensities was found. [29] The smoothing steps then enable derivative analysis to be applied in order to identify band centres and hence accurate spectral deconvolution into the contributing bands. Confidence in the deconvolution procedure arises firstly from the minimizing of the underlying spectral deviations from the FFT smoothing, and secondly because the derivative analysis identifies bands at well-known band frequencies reported in the literature.

Spectra were recorded and averaged (3–5 co-averages per point) over 10 different surface locations on a given cross-section corresponding to the macrofibrils and intermacrofibrillar matrix, showing good reproducibility both across different locations on the same cross-section as well as for different cross-sections corresponding to the same hair fibre. It was found that further averaging over more surface locations on a given sample made minimal changes to the average spectra due to the high reproducibility achieved. Some variability in the absolute spectral contributions from average spectra between cross-sections of different fibres was observed, which is to be expected for complex biological samples. However, the relative comparisons of average spectra between the macrofibrils and surrounding matrix were qualitatively consistent, leading to the same conclusions reported later. Due to the variability between fibres, the 'global average' relative intensities are not presented here as they contain disproportionately high uncertainties and are not representative of the qualitative differences observed for a given sample. Furthermore, as there is significant variability between different fibres, the analysis and conclusions presented here are based on qualitative comparisons of relative spectral intensities rather than on quantitative specific intensity data. Instead, the spectra and analysis presented here are from a representative fibre, with spectra averaged across multiple locations within a section and across several sections.

RESULTS

Figure 2 shows AFM-IR analysis of the cortical cell, displaying averaged individual point spectra corresponding either to the Ext-matrix regions or to macrofibrils, as well as AFM topography maps alongside maps at specific IR bands observed in the spectra from a representative cross-section. Band assignments from the literature are given in Table 1. The survey recordings of the AFM-IR spectral maps and point spectra show significant variation in the relative band intensities between the Ext-matrix and macrofibril regions on the surface. The maps at 1330, 1465 and 1736 cm^{-1} all show increased intensity for the macrofibrils and smaller contributions from the Ext-matrix, whereas all other mapped frequencies show the reverse, that is enhanced IR signal for the Ext-matrix and less for the macrofibrils. Although the spectral intensity is small, these variations are nevertheless confirmed in the spectra themselves which, although they have not been normalized, show larger relative contributions from the 1330, 1465 and 1736 cm^{-1} bands in the macrofibril averaged spectrum. The structural interpretation of the nine bands identified in Table 1 is presented below.

The assignments of the bands at 1330, 1465 and 1736 cm^{-1} given in Table 1 and the observed intensities in the AFM-IR spectra and maps in Figure 2 indicate that the macrofibril regions show greater contributions from C-H and carbonyl C = O carriers. Given their long hydrocarbon chain groups and their ester functionalities, lipid and triglyceride species would be expected to make significant

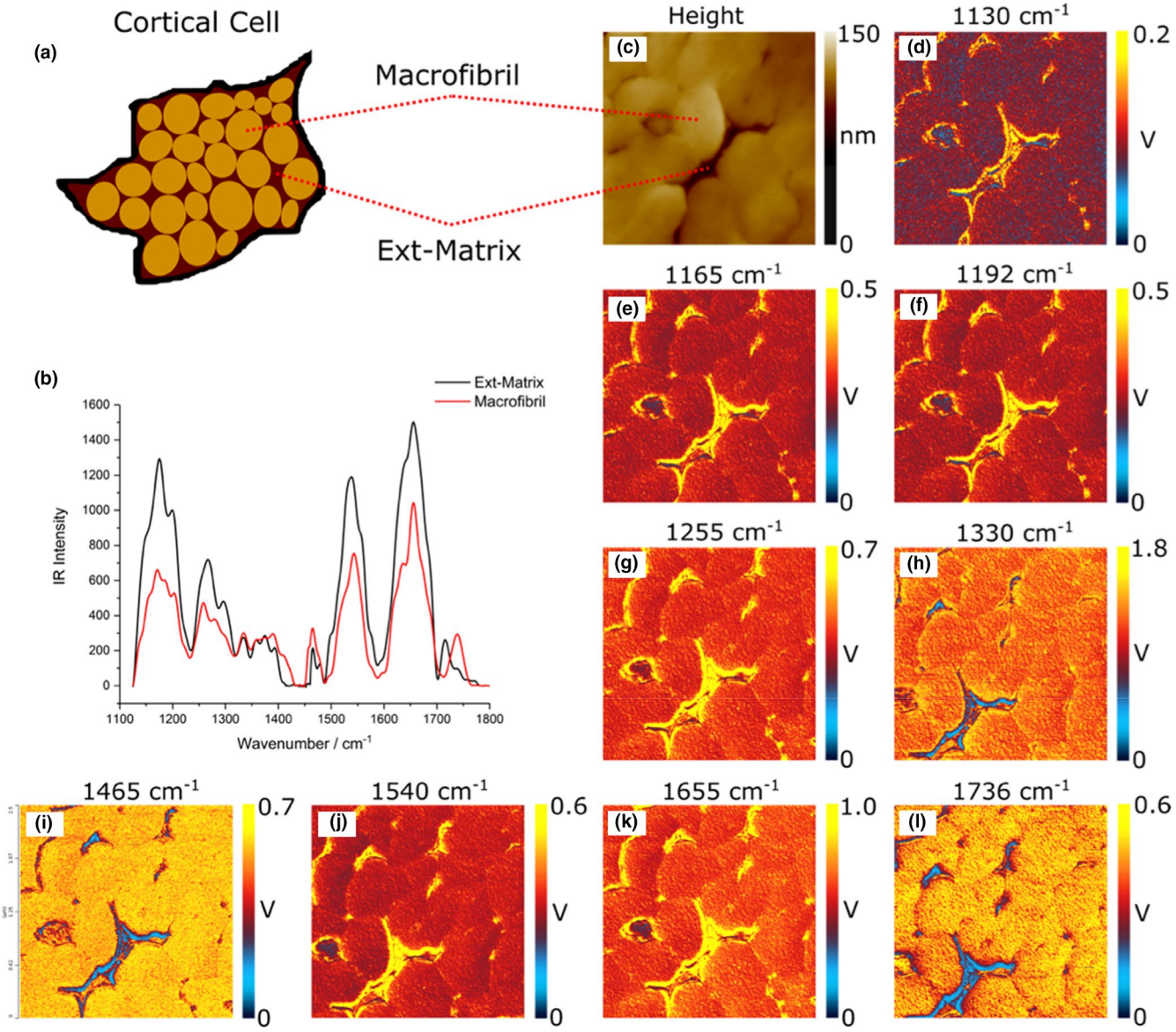

FIGURE 2 AFM-IR data obtained from a human hair cross-section (approx. 300 nm thick) showing (a) a schematic structural representation of the cortical cell (b) average spectra corresponding to each observed region (macrofibril and Ext-matrix) (c) AFM height map and (d)-(l) IR-intensity maps recorded in contact mode across a 2.5 × 2.5 μm region of the surface at a number of different infrared frequencies corresponding to contributions observed in the spectra (each shown above the corresponding image) for a representative fibre section

TABLE 1 Assignments of the bands observed in Figure 2 based on data reported in the literature.[31–38]

Band / cm^{-1}	Assignment
1130	SO_2 Stretch (Cysteine-Related Products)
1165	Asymmetric Cysteic Acid Stretch
1192	SO_2 Sulphonyl Chloride Stretch
1255	Amide-III
1330	C-H Twist / Wag
1465	CH_2 Scissor or CH_3 Asymmetric Bend
1540	Amide-II
1655	Amide-I
1736	Carbonyl C=O stretch

contributions to both the C-H and C=O spectral regions. However, it is well known that, in the human hair cortex, lipids and triglycerides are only present in significant quantities within the β-layers and the δ-layer, respectively, of the CMC, with most regions predominantly occupied by an abundance of proteinaceous material. [39–43] Because of this, even though proteins have relatively low hydrocarbon content (cf. lipids and triglycerides), it is reasonable to assume that the main contributor to the C-H backbone peaks at 1330 and 1465 cm^{-1} is proteinaceous in nature. More specifically, aliphatic amino acid residues such as leucine which are known to be highly prevalent in the hair cortex, [44,45] are likely to be significant sources of these bands.

Unlike the C-H contributions, however, most amino acids do not present with a carbonyl group above 1700 cm^{-1}. Only those with acidic side chains will give rise to higher carbonyl stretching frequencies >1700 cm^{-1}, for example glutamic acid (Glu) and aspartic acid (Asp) which are known to be the most prevalent and have carbonyl bands coinciding with observation. [44,45] Hence, the relative lipid and triglyceride contributions to this spectral region are expected to be significantly greater despite the low levels of lipids and triglycerides within the cortex. Additionally, the position of carbonyl bands above 1700 cm^{-1} is expected to vary due to the wide range of chemical environments and association states that can exist due to hydrogen bonding. This accounts for the broad carbonyl band above 1700 cm^{-1} appearing in the spectra in Figure 2 and which, interestingly, shows a different structure in the two areas investigated. To summarize, in the AFM-IR maps, all three bands assigned to C-H and C=O functional groups appear with greater intensity for the macrofibrillar regions; that is, there are greater concentrations of the carriers of these bands in these regions. However, the significant overlap of the bands means that IR mapping by analysing individual contributions is unreliable.

The bands at 1655, 1540 and 1255 cm^{-1} all source from predominantly protein-related species, being assigned to three amide bands. Although significant in both regions, their relative intensity is greater in the Ext-matrix. Similarly, the bands related to cysteine (Cys) derivatives at 1130, 1165 and 1192 cm^{-1} also have an increased intensity in the Ext-matrix cf. the macrofibrils. (Although the Cys bands can overlap with those from lipid and triglyceride C-O moieties, these modes should be significantly weaker due to their relative abundances, that is significant Cys in

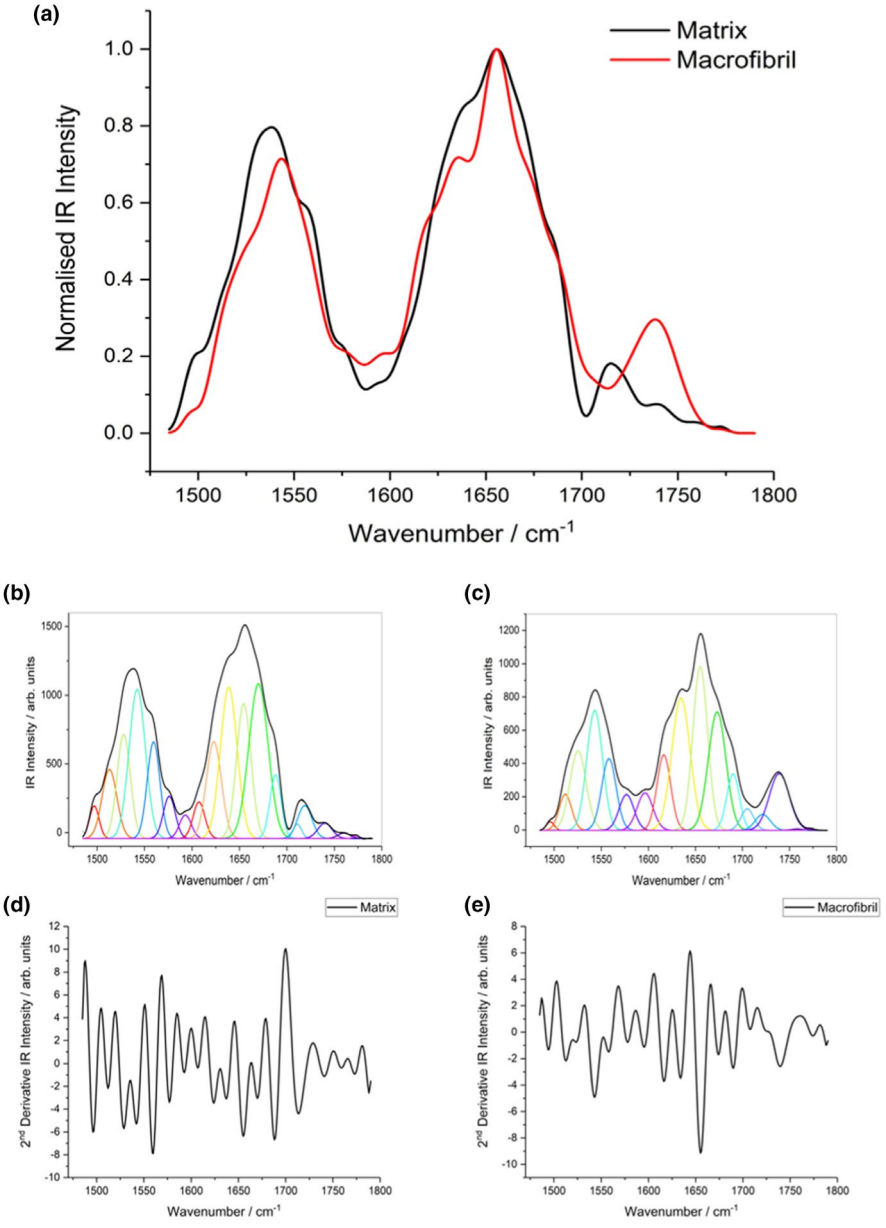

FIGURE 3 AFM-IR spectral analysis of the Ext-matrix and macrofibrils showing (a) overlapping spectra from 1470 to 1780 cm^{-1}, containing the Amide-I and Amide-II regions of the spectra shown in Figure 2, as well as individual deconvoluted spectra in this region for (b) the matrix and (c) the macrofibrils. The smoothed spectra were fitted using the contributing bands that were identified in the second-derivative spectra shown in (d) and (e) as described in the text

matrix material and lower lipids contributions within the matrix as mentioned earlier.)

The small band at ~1710 cm^{-1} in Figure 2 is present in the Ext-matrix and virtually absent in the macrofibril regions. This is just a shift in the band centred at 1736 cm^{-1} in the macrofibril spectrum can be discounted since this feature is also present in the Ext-matrix spectra but with much lower intensity. As already mentioned, C = O bands above 1700 cm^{-1} are expected to show significant variation in their positions due to large environmental shifts for the carbonyl carrying moieties. Therefore, the region >1700 cm^{-1} is expected to house several contributions from different carbonyl environments. It is reasonable to assign the band at 1710 cm^{-1} to contributions from acidic amino acid side chains with significant intermolecular H-bonding, well known to weaken the carbonyl bond and hence reduce the stretching frequency. The broader band centred at 1736 cm^{-1}, however, must arise from stronger carbonyl moieties, for example esters sourcing from lipids or triglycerides as well as acidic side-chain amino acids with less intermolecular association, that is stronger carbonyl bonds. From this analysis of the AFM-IR spectra for the two different regions, it is clear that there is a large variation in the carbonyl group environments and their states of association within the cortex region, with each component region exhibiting different relative contributions from each carbonyl environment. A more detailed discussion of these contributions follows below.

It is important to note that the IR mapping presented in Figure 2 does not lead to conclusive chemical analysis of the structures of interest owing to potential measurement artefacts that can arise due to tip-sample coupling and imperfect tracking across the surface. (In this case, the imperfect tracking effects appear to be minimal, as demonstrated by the low-intensity deflection map in Supplementary Information, Figure S2.) Additionally, there are intensity contributions that arise from resonances at nearby frequencies in the spectra. The latter point is particularly worthy of consideration given the highly convoluted nature of the Amide bands from proteinaceous material. It is, therefore, crucially important to analyse the observed structures using point spectra, where the highly convoluted bands can be deconvoluted, in order to characterize their chemical structure and constituents.

Since a significant proportion of the composition of hair is composed of protein, the contribution that they make to the macroscopic properties of hair fibres is of central importance. Hence, characterization of the protein structure in different regions has been of particular interest in much of the large amount of work reported to date. [5,44–48] Therefore, our attention was focussed on deconvoluting the Amide-I and Amide-II spectral region (1470–1780 cm^{-1}) with spectra smoothed with a 7-point FFT-filter to reduce noise and allow for second-derivative peak-finding. The resulting spectra within this region, along with their second derivatives, are shown in Figure 3.

From the fitted spectra, it is clear that there is a difference in the number of contributing bands in the two regions. The second-derivative plots show similar band centres for all contributing bands except the band at approximately 1616 cm^{-1}, which is missing in the Ext-matrix spectrum but replaced with two bands at 1607 and 1623 cm^{-1}, which are not present in the macrofibril spectrum. Since the separation of these bands lies outside the cut-off frequency of the FFT smoothing filter (7 cm^{-1}), either of these contributions in the macrofibril spectrum cannot source from the same species as those which give rise to the identified band in the matrix spectrum without cause for a significant band-centre shift. Furthermore, this also suggests a change in the number of clearly identifiable constituent protein structures. The observed bands for macrofibril and Ext-matrix are given in Table 2 where the observed differences between them are ≤4 cm^{-1}, that is within the uncertainty margin associated with the spectral resolution and subsequent 7pt FFT algorithm. Also, given are the assignments of the deconvoluted bands based on well-established data from the literature. [31,32,49–52] Figure 4 shows the constituent bands from the Ext-matrix and macrofibril spectra shown in Figure 3 presented in block format, that is representing the integrated band intensities. This demonstrates the clear spectral difference between the two regions, with 3 of the assigned bands only being present in 1 of the 2 spectra and the others showing relative intensity shifts. Because of the overlap of bands from different constituents, changes in local concentrations can generally only be deduced after deconvolution (an exception is the relatively well-resolved Cys-related band between 1125 and 1225 cm^{-1}). Bands in the Amide-I and Amide-II regions, identified by deconvolution using an FFT-filter and second derivative peak fitting, are given in Table 3 based on previously reported assignments in the literature. [30] This table identifies the substantial residues, and secondary structures revealed spectroscopically and consequently the regions showing the greater proportions of each.

DISCUSSION

To begin, we consider the information that can be deduced from the AFM-IR maps and average spectra presented in Figure 2. The spectra, averaged over several points on the surface in the regions of the macrofibrils and the Ext-matrix, and across different sections of the

TABLE 2 Contributions in the Amide-I and Amide-II spectral regions obtained by second-derivative peak fitting for each of the spectra shown in Figure 3

	Matrix	Macrofibril	Assignment
Band 1	1497	1496	His / Trp (C-N Str. in ring)
Band 2	1513	1512	β-Sheet (Antiparallel)
Band 3	1528	1525	β-Sheet (Parallel)
Band 4	1542	1543	α-Helix / Random Coil
Band 5	1560	1558	Trp (Indole ring vibration)
Band 6	1576	1577	Asp / Glu COO^- (Antisym Str.)
Band 7	1593	1596	His / Tyr / Trp (C-C Str. in ring)
Band 8	1607	-	β-Sheet (Antiparallel)
Band 9	-	1616	β-Sheet (Antiparallel)
Band 10	1623	-	β-Sheet (Antiparallel)
Band 11	1639	1635	β-Sheet (Parallel)
Band 12	1654	1655	α-Helix
Band 13	1670	1673	β-Turn
Band 14	1688	1690	Asn / Gln (Amide Str.) / higher β-Sheet
Band 15	1711	1705	C=O (Acidic Residues)
Band 16	1719	1721	C=O (Acidic Residues)
Band 17	1740	1739	C=O (Lipid / Triglyceride Esters)
Band 18	1760	1758	C=O (monomeric acid residues)
Band 19	1773	1773	C=O (monomeric acid residues)

same fibre, show significant differences in the relative intensities for the various bands. The macrofibril regions show higher intensity for the bands corresponding to C-H moieties (1330 cm^{-1} C-H twist / wag and the 1465 cm^{-1} combination of CH_2 scissoring and CH_3 asymmetric bending). The major contributions to the C-H band intensity are from the aliphatic amino acid residues in the proteinaceous material and from the lipid tail groups, due to a higher proportion of CH_2 groups compared with non-aliphatic protein species. The 1736 cm^{-1} band also shows a much-increased profile for the macrofibrils, but this is a result of overlapping bands from numerous species and environments making spectral deconvolution necessary for quantitative analysis. Similarly, those bands associated with Cys-related molecules that have S-O related stretches in the 1100–1200 cm^{-1} spectral region (cystine, cystine monoxide / dioxide, cysteic acid / sulphonyl chloride), as well as the generic protein-associated bands (Amide-I, -II and –III), which originate from all amino acid residues, all show an increased profile in the Ext-matrix compared with the macrofibrils regions. The spectral results are consistent with the known structure and composition of the Ext-matrix as being a highly proteinaceous region with considerable Cys content (high-sulphur keratin-associated proteins, KAPs) and minimal lipid presence.

At first, it might be assumed that the amorphous material constituting the Ext-matrix might have a lower protein density than the macrofibrils, which contain well-ordered intermediate filaments. However, the macrofibrils contain both intermediate filaments and Int-matrix, and hence, the protein content in them will be averaged over both species. The intermediate filaments are stabilized through significant H-bonding of the intramacrofibrillar material, and it is reasonable to assume that this results in an increased intermolecular spacing and a decreased density compared with the Ext-matrix. This follows with the observed increases in the IR maps corresponding to the Amide bands in the Ext-matrix regions. The lipid component of the macrofibrils, however, is found to be significantly greater than in the Ext-matrix, contrary to some previous suggestions that lipid can be pushed into inter-macrofibrillar material during the growth and hardening of the hair fibres. [28]

Any structural lipids that are bound within protein networks are more likely to remain within the Int-matrix where greater stabilization of the intermediate filament proteins can result, in agreement with the difference in lipid content between the two structures found here (although it should be mentioned that both have relatively low lipid contributions c.f. proteinaceous material). Leucine has been previously found to be a dominant amino acid in the hair cortex and to be in greater proportions in the intermediate filament proteins of the macrofibrils compared with the surrounding Ext-matrix, hence the enhanced C-H 1330 and 1465 cm^{-1} bands for the macrofibrils.

We next consider the structural results derived from examining the spectra comprising the Amide-I and II

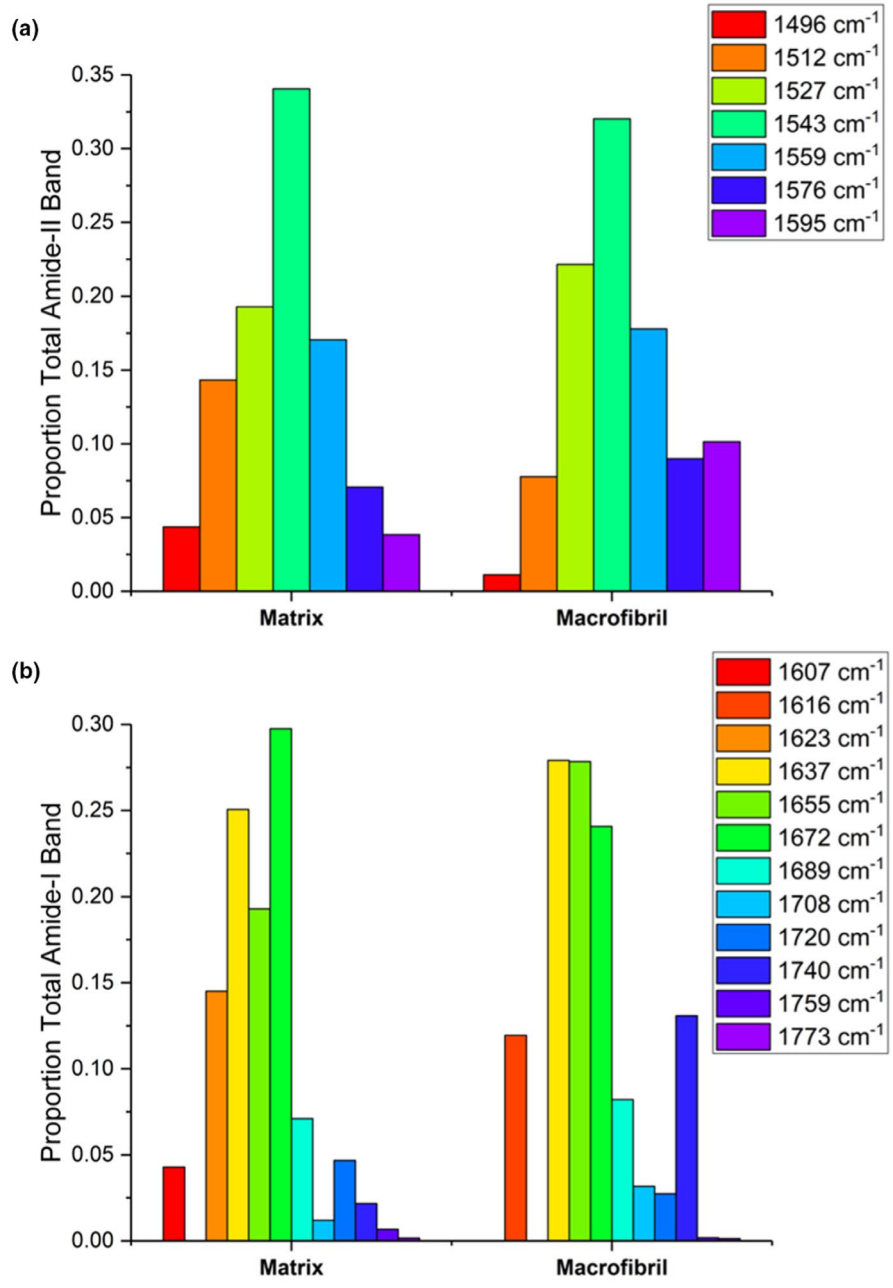

FIGURE 4 Deconvolution profiles calculated from the contributing band integrations shown in Figure 3; (a) Amide-II and (b) Amide-I

regions. In the Amide-I region, whereas the Ext-matrix shows bands at 1607 cm^{-1} (band 8) and 1623 cm^{-1} (band 10), there is only one band in this region in the macrofibril spectra at 1616 cm^{-1} (band 9). All three are assigned to antiparallel β-sheet structures and therefore must arise from a different arrangement of these secondary structures as noted previously by Litvinov et al. [53]. The band at 1616 cm^{-1} strongly suggests that the macrofibrils have different β-sheet structures with more intermolecularly H-bonded, aggregated protein. Given that the hair fibres are generally not under tension, the intermediate filaments will majoritively consist of α-helix protein structures, hence the β-sheet contributions most likely arise from the Int-matrix within the macrofibrils. The observed variation shows that the Int-matrix presents more intermolecularly H-bonded β-structures, whereas the Ext-matrix exists with both intramolecular β-sheet structures and some intermolecular H-bonding, but with significantly different aggregation structures. Band 11 (1635–9 cm^{-1}), associated with the parallel β-sheet secondary structure, shows a greater proportion from the macrofibril (Int-matrix) despite higher concentrations of overall β-sheet structures in the Ext-matrix. This illustrates the differences in the two types of matrix material: The Int-matrix is dominated by the less stable parallel β-sheets and β-sheets involved in intermolecular H-bonding interactions. Conversely, the Ext-matrix exhibits both strong intermolecular H-bonding and intramolecular interactions within its β-sheet structures which exist mostly in the antiparallel arrangement, consistent with a greater conformational and structural

TABLE 3 Summary of the contributing residues and secondary structures present in the hair cortex indicating the regions of greater band contributions. The abbreviations used are Mtx – Ext-matrix, MF – macrofibril (combined intermediate filament and Int-matrix)

Species	Contributing Bands	Greatest Contribution In
Cys	1130, 1165 and 1192 cm^{-1}	Mtx
His	1, 7	Mtx
Trp	1, 5, 7	Approx. Equal
Tyr	7	MF (within I-Matrix)
Deprotonated Asp / Glu	6	Approx. Equal
Amide side chain Asn / Gln	14	MF
H-bonded Acidic Asp / Glu	15	MF
'Free' Acidic Asp / Glu	16	Mtx
Monomeric Asp / Glu	18–19	Mtx
Asp / Glu (total)	6, 14–16, 18–19	MF
β-Sheet (AP)	2, 8, 9	Mtx
β-Sheet (P)	3, 10, 11	MF
β-Sheet (total)	2–3, 8–11	Mtx
α-Helix	4, 12	MF
Random Coil	4	Mtx
β-Turn	13	Mtx
Lipid / Triglyceride	17	MF

freedom within the Ext-matrix. In contrast, the network of proteins in the Int-matrix is more restricted and is believed to be due to the significant cross-linking from Cys-related species and stabilizing interactions between the Int-matrix and intermediate filaments. The Ext-matrix consists of homogeneous matrix material unlike the macrofibrils which are a combination of the Int-matrix and intermediate filaments. It is, therefore, expected that both types of matrix species will present high Cys-related proportions. The gel-like Ext-matrix is highly susceptible to water uptake and, despite having a high Cys content, is not expected to present significant cross-linking in contrast to the macrofibrils where cross-linking is thought to be more significant. This conclusion is compatible with the more restricted protein network observed within the macrofibrils as well as the greater intensity from the Cys-oxidation products which indicates Cys residues that are not undergoing cross-linking. The complementary α-helix secondary structures in these regions (band 12 at 1654–5 cm^{-1}) show that there is a greater contribution in the macrofibrils, as expected and consistent with their observed lower β-sheet contributions.

The final 3 bands below 1750 cm^{-1} (bands 15, 16 and 17) at 1705–11, 1719–21 and 1739–40 cm^{-1} all arise from higher carbonyl stretching modes, and the first two believed to be Asp and Glu residues. The band at 1739–40 cm^{-1} is due to ester moieties contributed by lipids and triglycerides that are relatively low in concentration in both species, consistent with the known structure of the cortex, but showing a greater relative concentration in the macrofibrils cf. the Ext-matrix. The higher frequency of the acid carbonyl group is due to 'free' -COOH groups and the lower to -COOH groups involved in significant intermolecular H-bonding. The higher frequency carries a greater contribution from the Ext-matrix, whereas the lower is more prevalent within macrofibrils. The α-helical structure of the intermediate filaments within the macrofibrils is known to be stabilized by H-bonding. [54,55] The amorphous Ext-matrix, on the contrary, has considerably less α-helical structured protein, for which band 12 is a marker, and hence will also have less propensity for these stabilizing H-bonds. The two bands above 1750 cm^{-1}, at 1758–60 and 1773 cm^{-1}, likely arise from monomeric acid side chains (i.e. Asp and Glu), as opposed to 'dimer-like' side chains, and are greater in the Ext-matrix than the macrofibrils. Both bands show small contributions in both regions compared with the 'dimer' counterparts, as would be expected in species where H-bonding in fairly unimpeded.

Next, turning to the Amide-II band, the lowest frequency feature at 1496–7 cm^{-1} corresponds to aromatic ring stretching modes of the indole or imidazole groups, dominated by tryptophan or histidine, with a greater intensity in the Ext-matrix. [44,49,50] The band at 1512–3 cm^{-1} arises from the antiparallel β-sheet secondary structure, also with higher intensity in the Ext-matrix, and is consistent with the antiparallel β-sheet bands found in the Amide-I regions. In contrast, the third contributing band at 1525–8 cm^{-1} arises from parallel β-sheet secondary structure and shows a greater intensity for the macrofibrils (also in agreement

with the Amide-I band deconvolution). The gel-like Ext-matrix facilitates easier rearrangement of molecules via hydrogen bonding, optimizing intermolecular interactions in comparison with the more restricted, cross-linked Int-matrix material that supports the intermediate filaments. [6,16–18] This difference in structural environments is compatible with the antiparallel β-sheet structures being more favoured in the Ext-matrix and the parallel form in the macrofibrils as previously suggested. Band 4 at 1542–3 cm^{-1} is believed to have contributions from both the α-helix and random coil secondary structures. To determine the relative contributions of each, we compared it with band 12 in the Amide-I region where it was found that, although the α-helix contribution to band 4 should mean an increased intensity for the macrofibril, the random coil contribution must be dominating and be greater in the Ext-matrix. This is consistent with the known structure since the intermediate filaments within the macrofibrils are known to be of high α-helix content when not under significant tension. [5,12–15] Band 5 at 1558–60 cm^{-1} has been found to be associated with tryptophan, and there is no significant difference in intensity between macrofibril and Ext-matrix, indicating a uniform contribution throughout. The band at 1576–7 cm^{-1} is an additional combination of Asp and Glu contributions (deprotonated) with greater intensity in the macrofibrils. This chimes with the other Asp and Glu contributions (bands 15 and 16) at higher frequencies and indicates no preference for the deprotonated form in either region. The observed relative proportions are just due to an overall concentration in the Asp and Glu residues, not a shift in the deprotonation equilibrium. Finally, the band at 1593–6 cm^{-1} arises from the C-C ring stretching modes of the dominant His, Try and Trp residues, again with a higher intensity in the macrofibril region, and the unknown relative contribution of each residue to the whole feature frustrates further analysis.

CONCLUSIONS

Survey spectrochemical mapping of cross-sections within the hair cortex using AFM-IR revealed significant regional differences in the contributing protein structures and amino acid residues, suggesting fundamental constituent differences between the intramacrofibrilar and intermacrofibrilar matrix materials. The macrofibrils exhibit greater proportions of aliphatic and acidic proteins as well as lipids and triglycerides whilst the surrounding matrix material shows much greater contributions from cysteine oxidation products and an overall greater protein concentration. Consistent with the presence of their constituent intermediate filaments, the macrofibrils showed greater relative proportions of α-helix protein than the surrounding intermacrofibrilar matrix, which conversely had greater proportions of β-structures. The β-sheet environments, since only in significant concentrations within matrix material (cf. intermediate filaments), provide a direct means for comparing the inter- and intramacrofibrillar matrix. The former showed significantly greater relative proportions of β-sheets in the more thermodynamically stable antiparallel configuration, whereas the parallel form was more prominent in the latter. It was concluded that the β-sheet structures exist in a more restrictive environment in the macrofibrils, inhibiting the thermodynamically favourable rearrangement, that could arise from cross-linking, for example due to H-bonding or disulphide linkages. This conclusion was supported by comparing the carbonyl stretching bands of the amide- or acid-containing side chains from the asparagine / glutamine and aspartic / glutamic acid amino acids, respectively, which showed greater overall relative proportions within the macrofibrils. Additionally, many spectral contributions are present from acid residues in the macrofibrils, arising from different association states of the -COOH group, indicating more significant H-bonding. Furthermore, the lipid contribution within the carbonyl region was also more significant (but still in relatively small amounts) within the macrofibrils, pointing to the presence of stabilizing structural lipids supporting the intermediate protein framework. Overall, the ability of AFM-IR to spectrally characterize these sub-diffraction limit components of the hair cortex has shed new light into their chemical distinction, showing fundamental differences between the inter- and intramacrofibrilar matrix materials.

ACKNOWLEDGEMENTS

We are grateful to Dr Paul Pudney and Dr Ken Lee at Unilever R&D for providing support and guidance through the project. Additionally, we are thankful for Unilever R&D and the EPSRC for providing the iCASE studentship for A. P. F. on Grant EP/R511870/1.

ORCID

A. P. Fellows https://orcid.org/0000-0002-5885-8144

REFERENCES

1. Dawber R. Hair: Its structure and response to cosmetic preparations. Clin Dermatol. 1996;14(1):105–12. doi:10.1016/0738-081X(95)00117-X
2. Bhushan B, Chen N. AFM studies of environmental effects on nanomechanical properties and cellular structure of human hair. Ultramicroscopy. 2006;106(8–9):755–64. doi:10.1016/j.ultramic.2005.12.010
3. Jones LN, Rivett DE. The role of 18-methyleicosanoic acid in the structure and formation of mammalian hair fibres. Micron. 1997;28(6):469–85. doi:10.1016/S0968-4328(97)00039-5

4. Pudney PDA, Bonnist EYM, Mutch KJ, Nicholls R, Rieley H, Stanfield S. Confocal raman spectroscopy of whole hairs. Appl Spectrosc. 2013;67(12):1408–16. doi:10.1366/13-07086
5. Robbins CR. *Chemical and physical behavior of human hair*, 5th edn. Berlin, Heidelberg: Springer-Verlag; 2012. doi:10.1007/9783642256110
6. Yu Y, Yang W, Wang B, Meyers MA. Structure and mechanical behavior of human hair. Mater Sci Eng C. 2017;73:152–63. doi:10.1016/j.msec.2016.12.008
7. Hashimoto K. The structure of human hair. Clin Dermatol. 1988;6(4):7–21. doi:10.1016/0738-081X(88)90060-0
8. Harkey MR. Anatomy and physiology of hair. Forensic Sci Int. 1993;63(1–3):9–18. doi:10.1016/0379-0738(93)90255-9
9. Hearle JWS. A critical review of the structural mechanics of wool and hair fibres. Int J Biol Macromol. 2000;27(2):123–38. doi:10.1016/S0141-8130(00)00116-1
10. De Cássia Comis Wagner R, Kiyohara PK, Silveira M, Joekes I. Electron microscopic observations of human hair medulla. J Microsc. 2007;226(1):54–63. doi:10.1111/j.1365-2818.2007.01747.x
11. Samanta A, Bhattacharya M, Dalui S, et al., Nanomechanical responses of human hair. J Mech Behav Biomed Mater. 2016;56:229–48. doi:10.1016/j.jmbbm.2015.10.010
12. Harland DP, Walls RJ, Vernon JA, Dyer JM, Woods JL, Bell F. Three-dimensional architecture of macrofibrils in the human scalp hair cortex. J Struct Biol. 2014;185(3):397–404. doi:10.1016/j.jsb.2014.01.010
13. Wilk KE, James VJ, Amemiya Y. The intermediate filament structure of human hair. BBA - Gen. Subj. 1995;1245(3):392–6. doi:10.1016/0304-4165(95)00111-5
14. Cao J. Is the α-β transition of keratin a transition of α-helices to β-pleated sheets. II. Synchrotron investigation for stretched single specimens. J Mol Struct. 2002;607(1):69–75. doi:10.1016/S0022-2860(01)00901-2
15. Kreplak L, Doucet J, Dumas P, Briki F. New aspects of the α-helix to β-sheet transition in stretched hard α-keratin fibers. Biophys J. 2004;87(1):640–7. doi:10.1529/biophysj.103.036749
16. Popescu C, Höcker H. Hair—the most sophisticated biological composite material. Chem Soc Rev. 2007;36(8):1282–91. doi:10.1039/b604537p
17. Shimomura Y, Ito M. Human hair keratin-associated proteins. J Investig Dermatol Symp Proc. 2005;10(3):230–3. doi:10.1111/j.1087-0024.2005.10112.x
18. Akkermans RLC, Warren PB. Multiscale modelling of human hair. Philos Trans R. Soc. A Math. Phys. Eng. Sci. 2004;362:1821, pp. 1783–1793. doi:10.1098/rsta.2004.1395
19. Dazzi A, Prater CB. AFM-IR: Technology and applications in nanoscale infrared spectroscopy and chemical imaging. Chem Rev. 2017;117(7):5146–73. doi:10.1021/acs.chemrev.6b00448
20. Perez-Guaita D, Kochan K, Batty M, et al., Multispectral Atomic Force Microscopy-Infrared Nano-Imaging of Malaria Infected Red Blood Cells. Anal Chem. 2018;90(5):3140–8. doi:10.1021/acs.analchem.7b04318
21. Ruggeri FS, Marcott C, Dinarelli S, et al., Identification of oxidative stress in red blood cells with nanoscale chemical resolution by infrared nanospectroscopy. Int J Mol Sci. 2018;19(9):1–14. doi:10.3390/ijms19092582
22. Fellows AP, Casford MTL, Davies PB, Gibson JS, Brewin JN, Rees DC. Nanoscale adhesion profiling and membrane characterisation in sickle cell disease using hybrid atomic force microscopy-IR spectroscopy. Colloids Surfaces B Biointerfaces. 2021;197: doi:10.1016/j.colsurfb.2020.111383. 111383.
23. Fellows AP, Casford MTL, Davies PB. Infrared Nanospectroscopy of Air-Sensitive Biological Substrates Protected by Thin Hydrogel Films. Biophys J. 2020;119(8):1474–80. doi:10.1016/j.bpj.2020.09.007
24. Ruggeri FS, Šneideris T, Chia S, Vendruscolo M, Knowles TPJ. Characterizing individual protein aggregates by infrared nanospectroscopy and atomic force microscopy. J vis Exp. 2019;2019(151):e60108. doi:10.3791/60108
25. Fellows AP, Puhan D, Casford MTL, Davies PB. Understanding the Lubrication Mechanism of Poly(vinyl alcohol) Hydrogels using Infrared Nanospectroscopy. J Phys Chem C. 2020;124(33):18091–101. doi:10.1021/acs.jpcc.0c04782
26. Vitry P, Rebois R, Bourillot E, et al., Combining infrared and mode synthesizing atomic force microscopy: Application to the study of lipid vesicles inside Streptomyces bacteria. Nano Res. 2016;9(6):1674–81. doi:10.1007/s12274-016-1061-6
27. Goussous SA, Fellows AP, Casford MTL, Davies PB. A time domain study of surfactin penetrating a phospholipid monolayer at the air-water interface investigated using sum frequency generation spectroscopy, infrared reflection absorption spectroscopy, and AFM-nano infrared microscopy. Biochim. Biophys. Acta - Biomembr. 2019;1861(9):1568–78. doi:10.1016/j.bbamem.2019.06.004
28. Marcott C, Lo M, Kjoller K, et al., Localization of human hair structural lipids using nanoscale infrared spectroscopy and imaging. Appl Spectrosc. 2014;68(5):564–9. doi:10.1366/13-07328
29. Fellows AP, Casford MTL, Davies PB. Nanoscale Molecular Characterization of Hair Cuticle Cells Using Integrated Atomic Force Microscopy-Infrared Laser Spectroscopy. Appl Spectrosc. 2020;74(12):1540–50. doi:10.1177/0003702820933942
30. Fellows AP, Casford MTL, Davies PB. Spectral Analysis and Deconvolution of the Amide I Band of Proteins Presenting with High-Frequency Noise and Baseline Shifts. Appl Spectrosc. 2020;74(5):597–615. doi:10.1177/0003702819898536
31. Barton PMJ. *A Forensic Investigation of Single Human Hair Fibres using FTIR-ATR Spectroscopy and Chemometrics*. Brisbane: Queensland University of Technology; 2011.
32. Panayiotuo H. *Vibrational spectroscopy of keratin fibers*. A forensic approach. School of physical and chemical sciences: Queensland University of Technology; 2004.
33. Kogelheide F, Kartaschew K, Strack M, et al., "FTIR spectroscopy of cysteine as a ready-to-use method for the investigation of plasma-induced chemical modifications of macromolecules". J. Phys. D. Appl Phys. 2016;49(8): doi:10.1088/0022-3727/49/8/084004
34. Dourado AHB, De Lima Batista AP, Oliveira-Filho AGS, Sumodjo PTA, Cordoba De Torresi SI. l-Cysteine electrooxidation in alkaline and acidic media: a combined spectroelectrochemical and computational study. RSC Adv. 2017;7(13):7492–501. doi:10.1039/c6ra26576f
35. Singh BR, DeOliveira DB, Fu F-N, Fuller MP. Fourier transform infrared analysis of amide III bands of proteins for the secondary structure estimation. Biomol Spectrosc. 1993;(1890):47–55. doi:10.1117/12.145242
36. Stanic V, Maia FCB, Freitas RDO, Montoro FE, Evans-Lutterodt K. The chemical fingerprint of hair melanosomes by infrared nano-spectroscopy. Nanoscale. 2018;10(29):14245–53. doi:10.1039/c8nr03146k

37. Nyquist R, "Sulfoxides, Sulfones, Sulfates, Monothiosulfates, Sulfonyl Halides, Sulfites, Sulfonamides, Sulfonates, and N-Sulfinyl Anilines". In: R. Nyquist, editors. *Interpreting Infrared, Raman, and Nuclear Magnetic Resonance Spectra*. Elsevier Inc.; 2001. p. 85–117. doi:10.1016/b978-012523475-7/50185-6
38. Bito K, Okuno M, Kano H, et al., Protein secondary structure imaging with ultrabroadband multiplex coherent anti-Stokes Raman scattering (CARS) microspectroscopy. J Phys Chem B. 2012;116(4):1452–7. doi:10.1021/jp210914x
39. Lyman DJ, Fay SG. The effect of breast cancer on the Fourier transform infrared attenuated total reflection spectra of human hair. Ecancermedicalscience. 2014;8:405. doi:10.3332/ecancer.2014.405
40. Robbins C. The cell membrane complex: Three related but different cellular cohesion components of mammalian hair fibers. J Cosmet Sci. 2009;60(4):437–65. doi:10.1111/j.1468-2494.2010.00577_6.x
41. Wolfram LJ. Human hair: A unique physicochemical composite. J Am Acad Dermatol. 2003;48(6 SUPPL.):S106–14. doi:10.1067/mjd.2003.276
42. Nogués B, Coderch ML, Erra P. Isolation and Partial Characterization of Glycolipids from Wool Fibers. Text Res J. 1986;56(9):588–90. doi:10.1177/004051758605600913
43. Hilterhaus-Bong S, Zahn H. Contributions to the chemistry of human hair: II. Lipid chemical aspects of permanently waved hair. Int J Cosmet Sci. 1989;11(4):167–74. doi:10.1111/j.1467-2494.1989.tb00506.x
44. Robbins CR. Chemical Composition of Different Hair Types. In: Robbins CR, editor. *Chemical and Physical Behavior of Human Hair*, 5th edn. Berlin, Heidelberg: Springer-Verlag; 2012. p. 105–76. doi:10.1007/978-3-642-25611-0_2
45. Robbins CR, Kelly CH. Amino Acid Composition of Human Hair. Text Res J. 1970;40(10):891–6. doi:10.1177/004051757004001005
46. Hu X, Cebe P, Weiss AS, Omenetto F, Kaplan DL. "Protein-based composite materials". Mater Today. 2012;15(5):208–15. doi:10.1016/S1369-7021(12)70091-3
47. Zhou Y, Rigoletto R, Koelmel D, Zhang G, Gillece TW, Foltis L et al., The effect of various cosmetic pretreatments on protecting hair from thermal damage by hot flat ironing. J Cosmet Sci. 2011;62(2):265–82.
48. Lyman DJ, Murray-Wijelath J, Feughelman M. Effect of temperature on the conformation of extended α-keratin. Appl Spectrosc. 2001;55(5):552–4. doi:10.1366/0003702011952343
49. Epishina LV, Slovetskii VI, Osipov VG, et al., Infrared spectra and the structure of salts of imidazoles. Chem Heterocycl Compd. 1969;3(4):570–5. doi:10.1007/BF00481609
50. Rao CNR, Venkataraghavan R. Contribution To the Infrared Spectra of Five-Membered N- and N, S-Heterocyclic Compounds. Can J Chem. 1964;42(1):43–9. doi:10.1139/v64-007
51. Kong J, Yu S. Fourier transform infrared spectroscopic analysis of protein secondary structures. Acta Biochim Biophys Sin (Shanghai). 2007;39(8):549–59. doi:10.1111/j.1745-7270.2007.00320.x
52. Barth A. Infrared spectroscopy of proteins. Biochim. Biophys. Acta - Bioenerg. 2007;1767(9):1073–101. doi:10.1016/j.bbabio.2007.06.004
53. Litvinov RI, Faizullin DA, Zuev YF, Weisel JW. The α-helix to β-sheet transition in stretched and compressed hydrated fibrin clots. Biophys J. 2012;103(5):1020–7. doi:10.1016/j.bpj.2012.07.046
54. Lehninger AL. Proteins: Three-dimensional Conformation. In: Lehninger AL, editor. *Biochemistry*, 2nd edn. New York: Worth Publishers Inc.; 1977. p. 125–55.
55. Cruz CF, Costa C, Gomes AC, Matamá T, Cavaco-Paulo A. Human hair and the impact of cosmetic procedures: A review on cleansing and shape-modulating cosmetics. Cosmetics. 2016;3(3):26. doi:10.3390/cosmetics3030026

SUPPORTING INFORMATION

Additional supporting information may be found in the online version of the article at the publisher's website.

How to cite this article: A.P. Fellows, M.T.L. Casford, P.B. Davies, Chemically characterizing the cortical cell nano-structure of human hair using atomic force microscopy integrated with infrared spectroscopy (AFM-IR). Int. J. Cosmet. Sci. 00, 1–14 (2021). doi:10.1111/ics.12753